

# Investigating the potential for a limited quantum speedup on protein lattice problems

Carlos Outeiral,<sup>1,2</sup> Garrett M. Morris,<sup>1</sup> Jiye Shi,<sup>3</sup> Martin Strahm,<sup>4</sup> Simon C. Benjamin,<sup>2,\*</sup> and Charlotte M. Deane<sup>1,†</sup>

<sup>1</sup>*Department of Statistics, University of Oxford,  
24-29 St Giles', Oxford OX1 3LB, United Kingdom*

<sup>2</sup>*Department of Materials, University of Oxford,  
Parks Road, Oxford OX1 3PH, United Kingdom*

<sup>3</sup>*Computer-Aided Drug Design, UCB Pharma,  
216 Bath Road, Slough SL1 3WE, United Kingdom*

<sup>4</sup>*Pharma Research & Early Development, F. Hoffmann-La Roche,  
Grenzacherstrasse 4058, Basel, Switzerland*

Protein folding, the determination of the lowest-energy configuration of a protein, is an unsolved computational problem. If protein folding could be solved, it would lead to significant advances in molecular biology, and technological development in areas such as drug discovery and catalyst design. As a hard combinatorial optimisation problem, protein folding has been studied as a potential target problem for adiabatic quantum computing. Although several experimental implementations have been discussed in the literature, the computational scaling of these approaches has not been elucidated. In this article, we present a numerical study of the (stoquastic) adiabatic quantum algorithm applied to protein lattice folding. Using exact numerical modelling of small systems, we find that the time-to-solution metric scales exponentially with peptide length, even for small peptides. However, comparison with classical heuristics for optimisation indicates a potential limited quantum speedup. Overall, our results suggest that quantum algorithms may well offer improvements for problems in the protein folding and structure prediction realm.

---

\*Electronic address: [simon.benjamin@materials.ox.ac.uk](mailto:simon.benjamin@materials.ox.ac.uk)

†Electronic address: [deane@stats.ox.ac.uk](mailto:deane@stats.ox.ac.uk)

## I. INTRODUCTION

The structure of a protein captures crucial information about its biological function and therapeutic potential [1]. Knowledge of a proteins' structure unlocks valuable biological information, ranging from the ability to predict protein-protein interactions [2], to structure-based discovery of new drugs [3] and catalysts [4]. Unfortunately, experiments to determine protein structure are challenging and require extensive time and resources [1, 5, 6]. As of February 2020, the TrEMBL database [7] contained 176 million protein sequences, while only 160,000 protein structures have been deposited in the Protein Data Bank [8]. A reliable computational algorithm for the template-free prediction of a protein's structure and its folding pathway from sequence information alone would enable annotation of millions of proteins and could stimulate major advances in biological research. However, despite steady improvements in the past six decades [9–11], a consistent and accurate protein folding algorithm has remained elusive.

Over the past decade, there have been attempts to leverage quantum computing for protein structure prediction. The biological structure of a protein is thought to correspond to the minimum of a free energy hypersurface, which for even small peptides is too vast for any classical computer to explore exhaustively [10]. A type of quantum computation that may be appropriate to help is adiabatic quantum computing (AQC), an approach to exploiting the physics of a controlled quantum system that is considered to be of potential use in optimisation problems (whether classical or quantum in nature) [12]. Typically, the set of possible solutions is mapped to a register of qubits with a binary encoding, and the objective function is represented as a physical Hamiltonian,  $H_{\text{problem}}$ , whose eigenvectors and eigenvalues are respectively problem solutions and their scores. In particular, the ground state  $|\Phi\rangle$  (or the respective ground eigenspace) corresponds to the global minimum of the problem. An adiabatic algorithm starts by initialising the register of qubits in the ground state  $|\Psi(0)\rangle$  of a given Hamiltonian,  $H_{\text{trivial}}$ , whose ground state is easy to prepare, and gently transforming into the problem Hamiltonian,  $H_{\text{problem}}$ . If the evolution is slow enough, the adiabatic theorem of quantum mechanics [13] ensures that the final state  $|\Psi(T)\rangle$  will be infinitesimally close to  $|\Phi\rangle$ .

Protein chemistry applications of quantum computing have concentrated on a simplified prototype known as the protein lattice model [14], which has been used as a coarse-grained

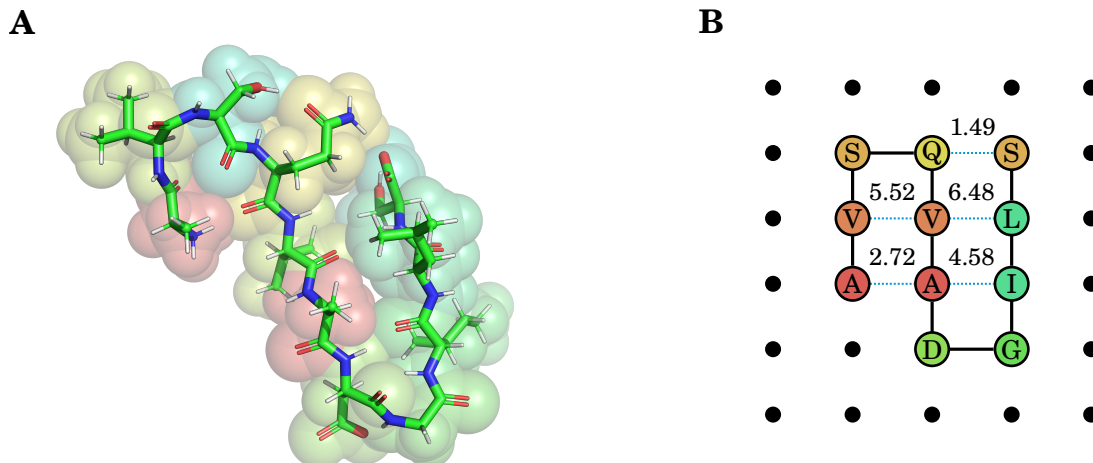


FIG. 1: (A) Liquorice representation of a randomly generated short protein (peptide) with sequence AVSQQVADGILS. In this depiction, every stick represents a bond between two atoms, and the colour of the corresponding half of the stick identifies the nature of the atom: green is carbon, white is hydrogen, blue is nitrogen and red is oxygen. The spheres that surround the sticks, representing van der Waals volume, have been coloured by residue identity. (B) Lattice model of the peptide in (A). The protein is represented as a self-avoiding walk on a lattice, where every node corresponds to a residue. Amino acids that are distant in the sequence but are spatial neighbours induce complex interactions (represented as dotted blue lines) that stabilise a particular fold. Above the dotted lines, we display the Miyazawa-Jernigan stabilisation energy of the contact.

proxy for structure prediction [15, 16]. In this model, the protein is described by a self-avoiding walk on a lattice, whose energy is determined by the contacts between adjacent amino acids, and the minimum energy is identified with the biologically active form of the protein. Unfortunately, the problem of finding the protein configuration that minimises the energy is known to be NP-hard [17, 18]. In the context of quantum computing, several encodings (*i.e.* instructions to map the problem to a Hamiltonian operator and the solutions to a binary string) have been proposed [19–21], some of which have also been tested experimentally in D-Wave processors [21, 22]. Recent work has attempted extensions of the protein lattice model [23], and even off-lattice models [24]. Although multiple algorithmic approaches have been suggested, there is not, to our knowledge, any numerical or analytical study establishing the computational scaling of adiabatic quantum computing for protein

folding applications.

In this article, we present an extensive numerical study of protein lattice folding in idealised, error-free, closed-system adiabatic quantum computing, such as might be achievable in future devices with long coherence times in the presence of error correction [25, 26], or with fault-tolerant universal quantum computers employing Hamiltonian simulation [27]. In particular, we have computed the minimum spectral gaps and optimised time-to-solution (TTS) metrics for a large dataset of hard problems. The spectral gaps display a strongly vanishing behaviour, which according to the adiabatic theorem leads one to anticipate a quadratically stronger upper bound in runtime. However, our simulations of unitary evolution reveal a scaling that is several orders of magnitude milder. When compared with classical stochastic optimisation heuristics, we find some evidence of a limited quantum speedup.

## II. RESULTS

We generated a large dataset of peptide (*i.e.* short proteins) problems with unique ground energy minima (UGEM) containing between 6 and 9 amino acids in 2D, and between 6 and 8 amino acids in 3D. We examined a total of 29,503 peptide sequences, an approximately equal number of cases in both dimensions (15,173 in 2D and 14,330 in 3D) and lengths (approximately 4,500 cases per length at a given dimension, with the exception of 2D length 7, where it is challenging to generate UGEM cases, and we considered only 1,700 cases).

These cases were generated by random sampling of the 20 standard amino acids, but are expected to display properties similar to realistic proteins, as established in several studies [28]. Using this dataset, we expressed the problems as Ising-like Hamiltonians by means of the turn circuit encoding described by Babbush et al. [20] and performed several numerical simulations to study the scaling of the minimum gap and time evolution.

### A. Spectral gap

We start our analysis by determining the minimum spectral gap,  $\Delta$ , between the ground state and the first excited state. It is often stated (based on theoretical arguments) that the runtime of the adiabatic algorithm is proportional to  $\mathcal{O}(\Delta^{-2})$  [29]. Unfortunately, many problems exhibit an exponentially vanishing gap with increasing problem size [30–32], and

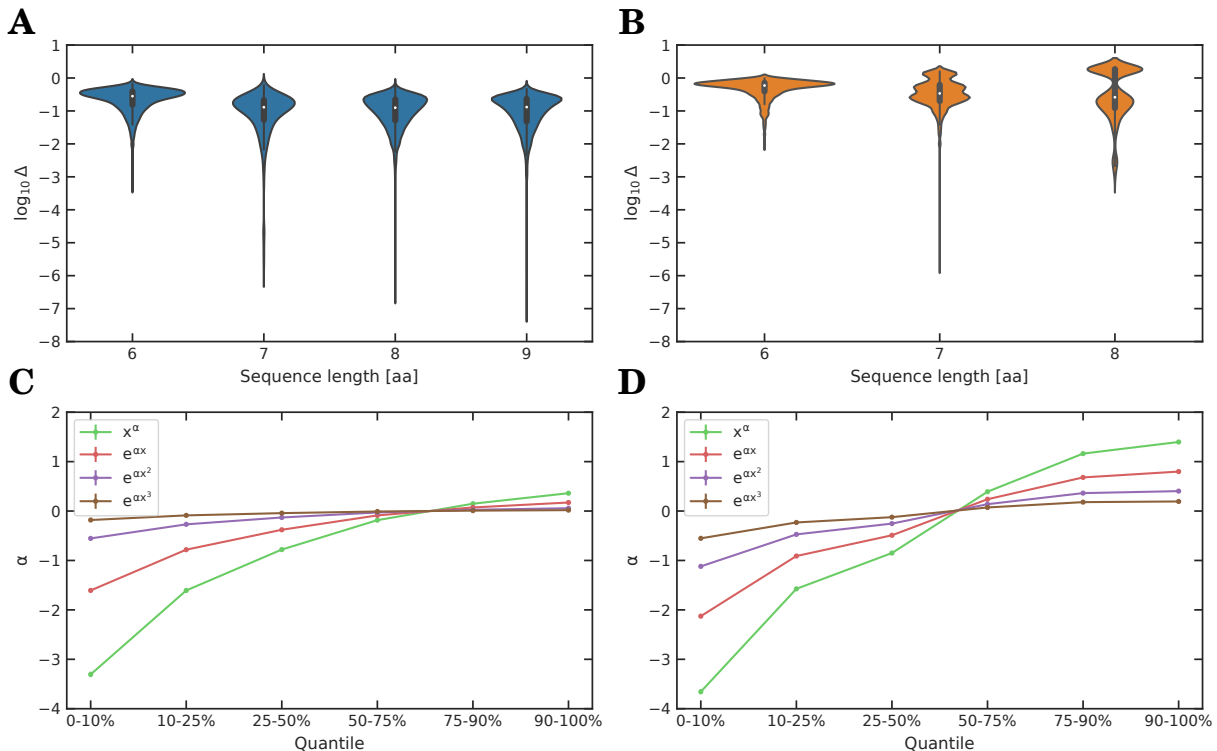


FIG. 2: (A, B) Distributions of  $\log_{10} \Delta$ , the decimal logarithm of the minimum spectral gap between the ground state and first excited state energy levels, for UGEM peptides of different size in 2D (A) and 3D (B). These violin plots employ a Gaussian kernel density estimation method to show a smooth representation of the distribution of data. In the 2D case (A), it is clear that the median gap remains approximately constant, while the worst case gap grows exponentially. In the 3D case (B), a similar effect is observed, although it is made less clear by the particular behaviour of length 8 peptides, which always have their optimal structures arranged in a cube. (C, D) Least-squares fit of subsamples of the data to different functional models. The rate of decay of the minimum spectral gap varies significantly between quantiles.

in particular it is believed that no form of quantum computing is able to efficiently solve NP-complete problems, or at least no such report has withstood scrutiny [29, 33]. The distribution of gaps for the protein lattice problem in 2D and 3D is shown in Figure 2.

The distribution of gaps at a given length resembles a skewed Gaussian distribution: the majority of gaps are concentrated around a narrow center spanning two orders of magnitude, and there are long, thick tails (containing 5-10% of the data) that spread away several

more orders of magnitude to one side. The extent of these tails present a severe decrease. In the dataset of 2D peptides, the size of the worst-case gaps decrease by five orders of magnitude within a length increase of four amino acids, but only an order of magnitude and a half within the last three lengths considered. Similar results are seen for the 3D peptides. Length 8 three-dimensional peptides show smaller gaps because of their distinct distribution of energetic levels due to cubic symmetry.

This steep decline for the hardest instances is in contrast with the small decrease experienced by an average peptide. The vast majority of the examples populate the area around the median gap, exhibiting a steady but far slower decline. A close examination of the violin plots for the 2D examples also reveals that the position of the peak of the distribution tends to rise as the sequence length increases, and in fact, if we ignore the tails of the distribution, the average gap increases rather than decreases. In interpreting this finding, it is important to keep in mind that our dataset is composed of peptide folding problems that are hard by design, since they have only one ground state solution (plus, in some cases, symmetry-equivalent configurations). These problems are known to be classically very hard [17, 18]. In addition to the lack of structure of NP-hard problems, the proportion of lowest-energy solutions in the solution space is minimal, so randomised algorithms will find it very challenging to find the ground state.

We characterised the scaling of the gap using regression analysis by Maximum Likelihood Estimation (see Methods for details). Four functional forms were considered: polynomial,  $x^\alpha$ , exponential,  $e^{\alpha x}$ , square exponential,  $e^{\alpha x^2}$  and cubic exponential,  $e^{\alpha x^3}$ . We then employed several standard model selection criteria, detailed in Appendix A, to select the model that better explains the data. The polynomial model  $x^\alpha$ , with  $\alpha \approx -0.75$  in 2D and  $\alpha \approx -0.4$  in 3D, is selected by all criteria, and is significantly better than the second best model.

We also binned the data into different quantiles and repeated the inference, to account for the inhomogeneity of the results (see Tables II and III in Appendix A). In 2D, the polynomial model is consistently selected across all quantiles, and in 3D, there are some quantiles where the exponential and cubic exponential are selected, which is probably due to the limited range of the dataset and the symmetry effect discussed above. We observed a notable variation of the coefficients across quantiles, as depicted in Figures 2C and 2D. For example, the first quantile, 0-10%, with  $\alpha = -3.23$  in 2D and  $\alpha = -3.65$  in 3D for the polynomial model, contains examples whose gaps vanish at a notably larger rate. On

the other hand, the two upper quartiles (75-90% and 90-100%) display positive  $\alpha$  values, showing that the gap actually widens with increasing size. Only a portion of the problem instances exhibits fast gap vanishing.

This data does not allow us to conclude that the gap vanishes polynomially. Our results are reminiscent of a previous study on the Exact Cover problem by Young et al. [34, 35]. In that study, it was described that, while the scaling of the spectral gap at small problem sizes is consistent with a polynomial [33], at large problem sizes the scaling turns exponential. Similarly, the fraction of problem instances exhibiting small gaps increases at large problem size [35]. We have been unable to study the behaviour of the protein lattice problem at greater sizes, given the large number of qubits and the difficulty of obtaining Hamiltonian expressions beyond 9 amino acids. However, we hypothesise that the protein lattice problem presents exponentially vanishing spectral gaps that will hinder a polynomial-time solution by quantum annealing.

### B. Zero-temperature simulations

The minimum spectral gap imposes an upper bound on the running time of the adiabatic algorithm, but in order to understand the behaviour of the process we need to access the evolution of the quantum state during the computational process. The numerical integration of the Schrödinger equation is costly, making the assessment of our entire dataset of *circa* 30,000 peptides beyond our resources. Instead, we selected two samples based on spectral gap values. The first sample contains the set of peptides with the smallest gaps (worst-case set), while the second sample is a random selection of peptides (random set). In both cases, each sample contains 100 peptides per chain length of a given dimension, giving a total of 1,400 instances.

A comparison of this sort requires optimising the annealing time to maximise the probability of success. As described by Rønnow et al. [36], a short run can provide a small, but sizeable probability that can be amplified by repetition. In many cases, the repetitions amount to a much shorter runtime than a longer, quasi-adiabatic runtime. We employed Bayesian optimisation [37, 38] to find the optimal runtime, as detailed in the Methods section. The optimised time-to-solution metric, corresponding to the expected runtime to find the correct solution with probability 50%, is shown in Figure ??A.

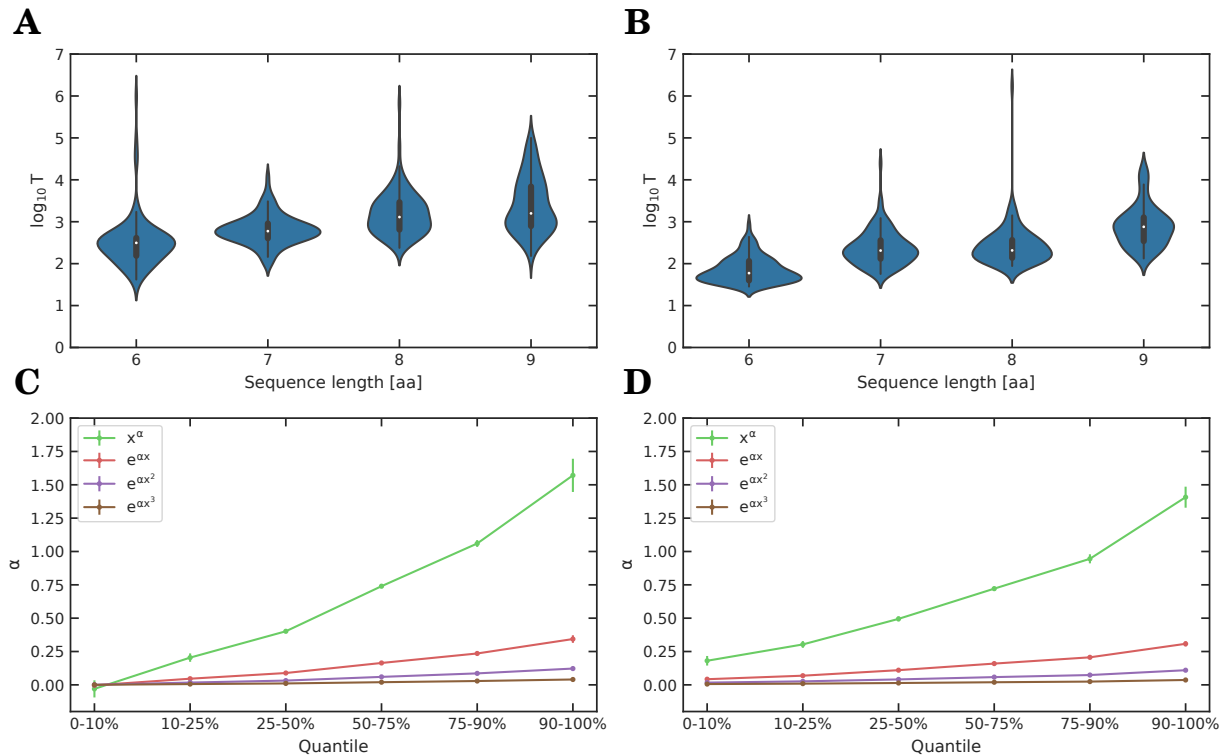


FIG. 3: (A, B). Distributions of the expected quantum annealing runtime  $T$  of the worst-case (A) and random (B) 2D sets. (C, D). Least-squares fit of subsamples of the data to different functional models for the worst-case (C) and random (D) sets.

The optimisation of the annealing time of an individual run has a significant impact. We simulated a baseline experiment in which the quantum annealer was run for 1000 a. u., and found an average improvement in the expected total runtime of 15 orders of magnitude in 2D and 10 orders of magnitude in 3D. We also find a small, but appreciable difference on the dependence on the gap, as depicted in Table I.

For both the 2D and 3D peptides, the worst-case set containing the smallest gaps does not require significantly longer expected runtimes than the random set. We performed a two-tailed Welch's  $t$  test, and found that the random and worst-case sets could not be distinguished ( $p$ -value 0.34, average  $p$ -value of subgroup analysis 0.31). In other words, the fact that a problem presents a very small minimum spectral gap does not necessarily indicate it will require a long runtime. This apparently contradictory statement might be explained by the fact that the  $\mathcal{O}(\Delta^{-2})$  scaling in relation to the spectral gap refers to the perfectly adiabatic algorithm, while in practical terms it is not necessary to guarantee that the final



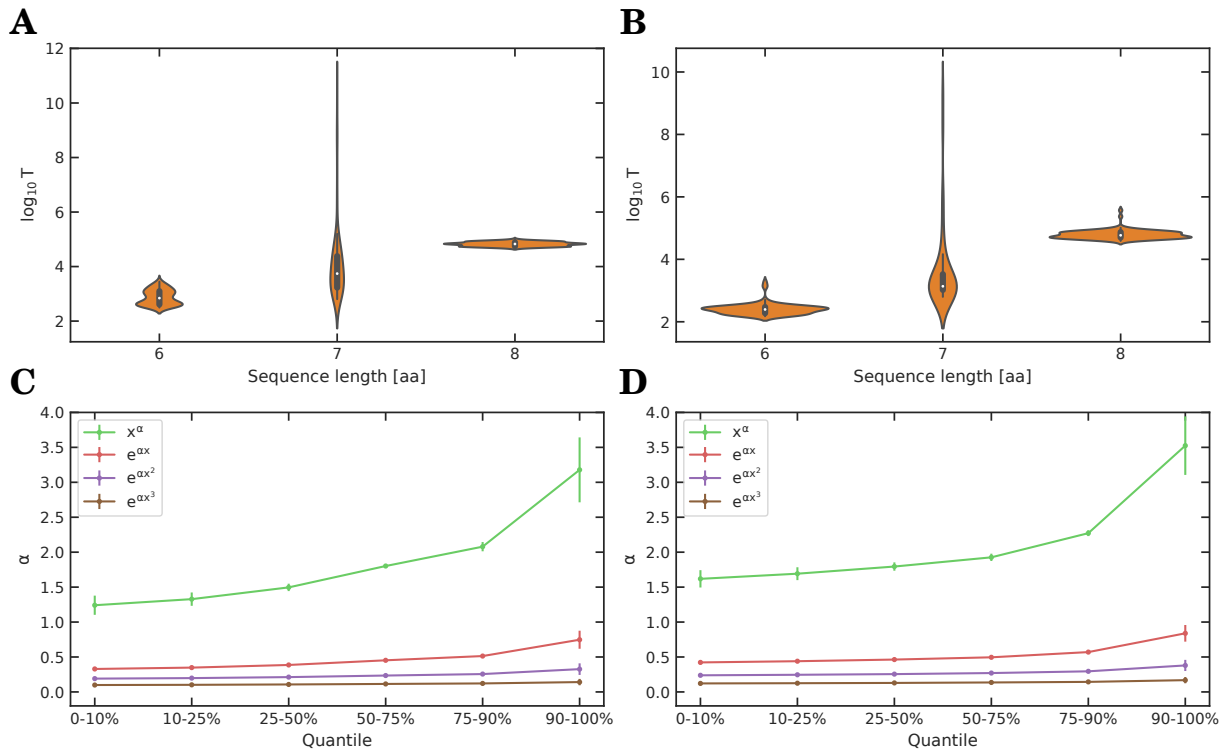


FIG. 4: (A, B). Distributions of the expected quantum annealing runtime  $T$  of the worst-case (A) and random (B) 3D sets. (C, D). Least-squares fit of subsamples of the data to different functional models for the worst-case (C) and random (D) sets.

state has a large fidelity with the ground state, but rather to ensure that it has a sizeable amplitude in order to obtain the expected result after enough trials. Another possibility to note is that within the range of problem sizes we inspect there may be only one (or a few) instances of the minimum (or near-minimum) gap occurring during the adiabatic sweep, whereas for large problems a near-minimum gap may occur at multiple points. In addition, the decrease by five orders of magnitude in 2D gaps discussed earlier is also markedly absent from Figures 3A and 3B.

We performed a scaling analysis identical to the previous section, finding that, for all cases, either the exponential model is selected over the polynomial, or there is not a significant difference between both of them (see Tables IV to VII in Appendix A). In particular, in 2D the polynomial model  $x^\alpha$  (with  $\alpha \approx 0.65$ ) and the exponential model  $e^{\alpha x}$  (with  $\alpha \approx 0.15$ ) cannot be separated. In 3D, an exponential model  $e^{\alpha x}$  with  $\alpha \approx 0.45$  is selected with high significance.

Our findings suggest that the protein lattice problem is not as severely affected by the

	$\rho$ 2D	$\rho$ 3D	$R$ 2D	$R$ 3D
Optimised time	-0.66	-0.44	0.52	0.38
Baseline	-0.73	-0.34	0.62	0.30

TABLE I: Correlation coefficients between expected runtime and gap, for the results obtaining optimising the individual runtime and the results obtained with a fixed runtime of 1,000 a.u.  $\rho$  is Spearman’s rank correlation coefficient between  $\Delta$  and  $T$ , which describes the monotonic relationship between the two variables ( $\rho = +1$  is perfectly monotonic,  $\rho = -1$  is perfectly inverse monotonic).  $R$  is Pearson’s correlation coefficient between  $\log_{10} \left( \frac{1}{\Delta^2} \right)$  and  $\log_{10} T$

vanishing of the spectral gap, as might have been expected. Problems with gaps smaller than  $10^{-2}$  a.u. (and down to  $10^{-8}$  a.u.) do not take significantly longer than problems with a median gap of 0.22 a.u. Moreover, we have established that the adiabatic algorithm displays an exponential scaling, albeit with a small rate constant. This analysis suggests that the adiabatic algorithm has a milder scaling than previously expected.

### C. Comparison with simulated annealing

We have observed that quantum annealing requires exponentially growing runtimes to find the ground state of a protein lattice model, even in the small range of lengths explored in our dataset (see Figures 3 and 4). Assuming this remains true of larger systems, as one would expect, it precludes an exponential speedup, since enumerating all possible conformations of a lattice model has the same asymptotic complexity. However, an algorithm which scales significantly better, that is, with a far smaller exponential rate  $\alpha$  than the classical case could still be useful for practical applications.

In this section, we compare quantum annealing with classical simulated annealing using the data displayed in Figures 5 and 6. Unlike other comparisons of quantum annealing and classical simulated annealing (*e.g.* [39]), we have not constrained the classical approach to solve a problem in the Ising form. More importantly, we consider a NP-hard problem, as opposed to previous work by Albash et al. [39] that considered simpler problems.

The distributions presented in Figures 5B and 6B show a rapidly growing number of

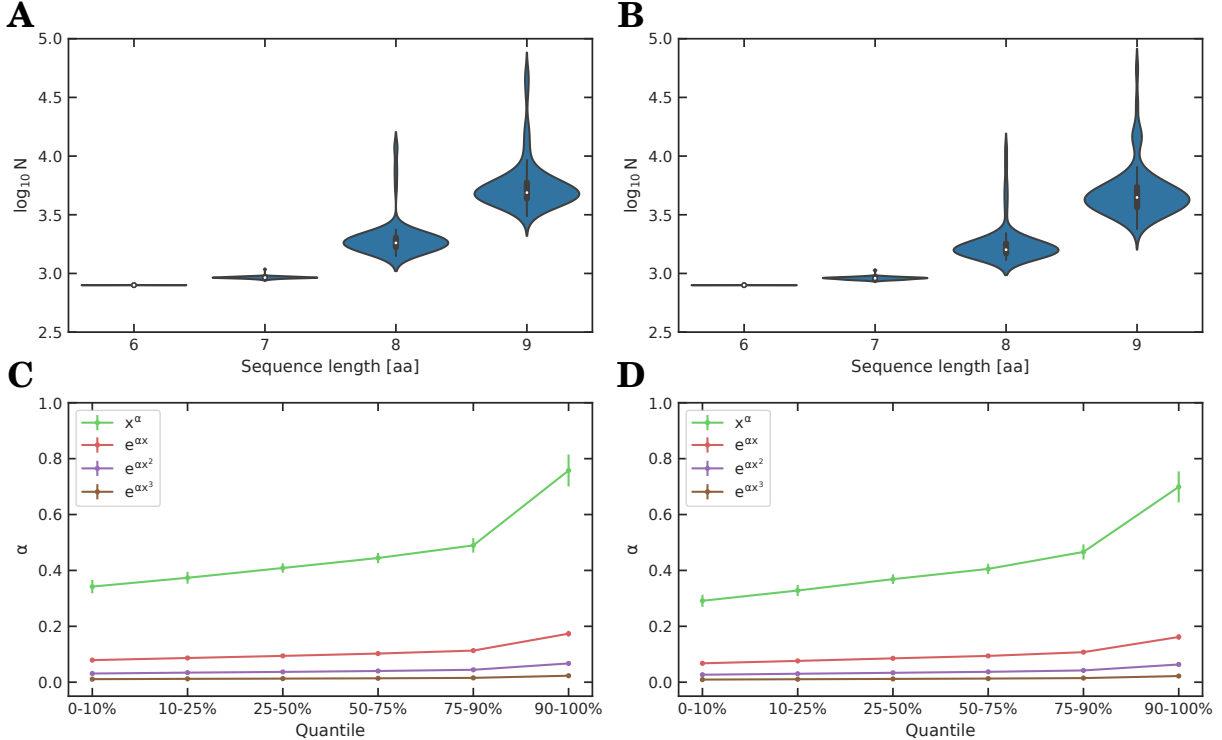


FIG. 5: (A, B). Distributions of the expected classical simulated annealing number of evaluations  $N$  of the worst-case (A) and random (B) sets. (C, D). Least-squares fit of subsamples of the data to different functional models for the worst-case (C) and random (D) sets.

evaluations. Visually, the runtime appears to display worse-than-exponential growth. Our model comparison analysis (see Tables VIII to XI in Appendix A) finds that, in all cases, the model fits to a square exponential  $e^{\alpha x^2}$  with a high level of significance (and this behaviour is reproduced at every quantile).

There are some theoretical arguments (e.g. [40]) which conjecture that simulated annealing converges in exponential time. The square exponential fit found by our statistical analysis could be an artifact of parameter optimisation (note that we optimise four parameters for a single simulated annealing run, as opposed to only one in quantum annealing). This anticipates that quantum annealing provides a better scaling. Our results are made stronger by the fact that in this analysis we have considered only the number of evaluations of the energy function; however, the cost of evaluating this energy increases with growing length.

These findings suggest that quantum annealing has an improved performance over sim-

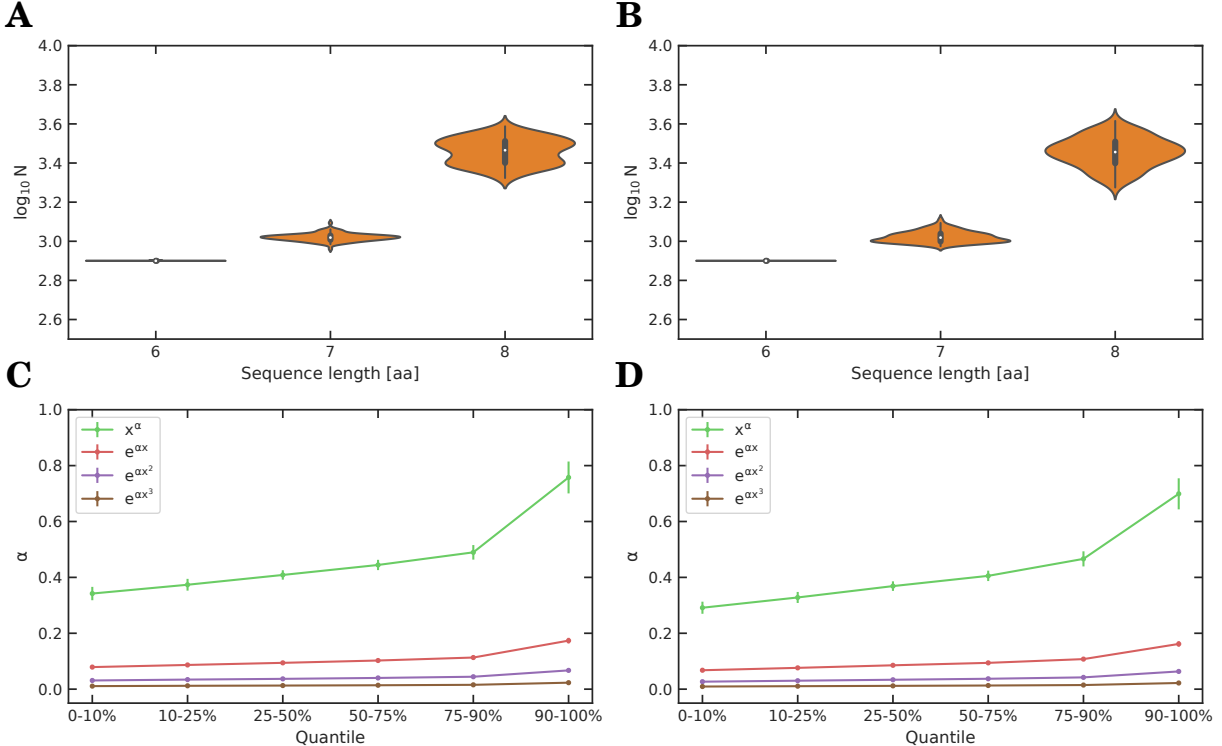


FIG. 6: (A, B). Distributions of the expected classical simulated annealing number of evaluations  $N$  of the worst-case (A) and random (B) sets. (C, D). Least-squares fit of subsamples of the data to different functional models for the worst-case (C) and random (D) sets.

ulated annealing. Over the system sizes we examined, the runtime of quantum annealing scales approximately exponentially, while simulated annealing shows a rapidly growing function that fits better to a double exponential.

### III. DISCUSSION

In this article, we have presented a numerical investigation of the adiabatic quantum algorithm applied to protein lattice models. We have considered nearly 30,000 protein sequences, each with a unique global energy minimum, which represent realistic protein problems displaying a folded state, but are also high difficulty instances of a NP-hard problem.

We first turned our attention to the minimum spectral gap, a quantity connected theoretically to the runtime of a perfect adiabatic computer. We have observed that the gap for these protein sequences can decrease quickly in magnitude, although the scaling appears

to be polynomial in the range of sizes considered. The polynomial scaling was confirmed by several statistical selection criteria (detailed in the Methods section and Appendix A), although comparison with prior results reported in the literature leads us to hypothesise that the gap vanishes exponentially. We have also observed that the worst cases decrease by five orders of magnitude between 6 and 9 amino acids. This numerical evidence shows that adiabatic evolution of the computer, where the probability of success nears 100%, will require rapidly growing runtimes and likely be infeasible for worst-case problems.

We then considered optimal adiabatic runs, where the computer is run for a shorter time to produce a small, but sizeable probability of success that is amplified by repetition. We have established that this runtime grows exponentially with peptide length, although the rate of growth was far smaller than the gap analysis suggested. This exponential rate was found to be approximately equal to 0.15 for 2D examples and approximately 0.75 for 3D instances. We also found statistical evidence that peptides with very small gaps are not significantly harder than average cases, and that the exponential rates are almost identical for these two datasets.

A comparison with classical simulated annealing on our dataset shows that the adiabatic algorithm is preferable. Statistical modelling seems to suggest that the scaling of simulated annealing fits best to a square exponential,  $e^{\alpha x^2}$  although theoretical arguments lead us to expect this behaviour to become exponential with a large rate as problem size increases. This implies that for large peptide sizes, an adiabatic quantum computer may take significantly less time than a classical machine running a stochastic algorithm.

One of the reasons why quantum annealing may prove useful for protein folding and structure prediction is the limited size of interesting problems. More than half the structures deposited in the Protein DataBank contain fewer than 500 residues, and 80% of the domains in the CATH database [41] are smaller than 200 residues. Similarly, the average length of a human protein (from sequences deposited in NCBI) is 480 amino acids. Even if the scaling of quantum annealing is exponential, as long as the exponential rate is low enough to fold small proteins or domains in a timely fashion, this approach will be useful for a multitude of practical problems.

There are other advantages to quantum annealing that could be explored further. When the adiabatic algorithm fails, the system has been excited to a higher energy state, but although this will only be a local minimum, it may still be useful. For example, if this result

is used in a bottom-up approach to explore the conformational space of a protein, it may still be a good starting point for more complex simulations. In contrast, classical simulated annealing is not guaranteed to provide a solution that is close to the global minimum.

We believe these results suggest that adiabatic approaches to quantum optimisation may be a powerful heuristic approach to solve the protein lattice problem. The difficulties of the quantum approach are shared by the classical simulated annealing approach, while the scaling is better. Moreover, even in cases where the adiabatic approach fails, it can provide solutions that despite not being equivalent to the global minimum, are very close to it, and may be useful in a subsequent refinement procedure. These findings offer encouragement for further research in quantum protein lattice folding and other hybrid quantum-classical algorithms for protein structure prediction.

## IV. METHODS

### A. Problem instance generation

Small peptide sequences with a unique global energy minimum (UGEM) have been shown to display the properties of real proteins [28]. To produce a large dataset of UGEM problem instances, we generated protein sequences by random sampling with replacement of the 20 standard amino acids (ARNDCQEGHILKMFPSTWYV). The states of these instances were enumerated by a brute force algorithm, scoring the energies using the Miyazawa-Jernigan 20-amino acid model [42], and all the sequences with two or more non-equivalent minimum energy conformations were rejected.

These sequences have to be mapped to an algebraic expression representing the couplings between individual spins in a programmable Ising model. This expression is often known as a Polynomial Unconstrained Binary Optimisation (PUBO) [43]. We employ here the *turn encoding* approach by Babbush et al. [20], which displays the highest reported efficiency in the number of qubits. We employed a modified version of *SymEngine* [44], a computer algebra system (CAS) developed in C++, to build the Hamiltonians. This modified version exploits the idempotency of binary variables leading to up to a five orders of magnitude speedup.

The code used to produce these Hamiltonians, as well as the modified version of

*SymEngine*, are available at <https://github.com/couteiral/proteinham>.

## B. Gap evaluation

We studied the protein Hamiltonians using numerical diagonalisation. An arbitrary Hamiltonian can be represented by a  $2^N \times 2^N$  matrix, which can reach several terabytes for some of the peptides in our study. However, every annealing trajectory in this study can be represented by a time-dependent operator of the form:

$$H(t) = \left(1 - \frac{t}{T}\right) H_{\text{start}} + \frac{t}{T} H_{\text{protein}} \quad (1)$$

$$H_{\text{start}} = \sum_{i=1}^N (I - \sigma_i^x) \quad (2)$$

where  $T$  is the total annealing time,  $I$  is the identity operator in the  $N$ -spin space *i.e.*  $I = I_1 \otimes I_2 \otimes \dots \otimes I_N$ ,  $\sigma_i^x$  is the Pauli X matrix applied to the  $i$ th spin in  $N$ -spin space, *i.e.*  $\sigma_i^x = \bigotimes_{k=1}^{i-1} I \otimes \sigma_x \otimes \bigotimes_{k=i+1}^N I$ , and  $t$  is the instantaneous time, the independent variable. For convenience, since energy levels do not depend on annealing speed, we define the annealing progress  $s = \frac{t}{T}$ . The choice of annealing trajectory is motivated by early proposals [12], and is the only available trajectory in D-Wave processors [45]. The relative disadvantage of stoquastic Hamiltonians of the form in equation 2 has been discussed elsewhere [29, 46, 47].

The annealing trajectory defined by equations 1 and 2 can be represented by matrices whose sparsity grows as  $\mathcal{O}(2^N)$ . Sparse matrix methods allow improvements of three to four orders of magnitudes in memory usage. We used the Krylov-Schur method [48, 49], as implemented in the *SLEPc* package [48, 50], to calculate the eigenvalues at different times of the annealing trajectory. We computed the eigenvalues in increments of 0.1 units, and interpolated the results using cubic splines. The gap was found as the minimum energy difference between every curve that ran into the ground state at the end of the evolution, and any other curve.

## C. Quantum annealing simulation

We simulated an idealised quantum annealer at zero temperature, in the absence of noise, and with perfect control over couplings. This was achieved by numerical integration of the

time-dependent Schrödinger equation:

$$\frac{d|\Psi\rangle}{dt} = -iH(t)|\Psi\rangle \quad (3)$$

were,  $H(t)$  is the time-dependent Hamiltonian defined in equation 1. We integrated this equation using the Runge-Kutta 5<sup>th</sup> order method with adaptive timestepping, as implemented in the *PETSc* package [51, 52]. Runge-Kutta methods have been previously validated for studying adiabatic evolution [53]. At the end of the evolution, the final state  $|\Psi(t = T)\rangle$  is a vector of amplitudes  $\Psi_i$  whose square modulus  $|\Psi_i^2|$  is the probability of measuring a particular binary string in the device.

Several authors have attested the need to use optimal time-to-solution (TTS) metrics to assess the scaling of an adiabatic algorithm, *e.g.* [36, 39]. We employed the Bayesian optimisation package *GPyOpt* [38] to optimise the annealing time  $T$ . We defined an optimisation domain between 0.1 and 1,000 a.u., which was considered acceptable after initial exploration, and ran the algorithm for a maximum of 50 iterations. Default parameters were used otherwise.

#### D. Classical simulated annealing

We implemented an energy routine in C++ and tested it against several manual examples. We employed the `gsl_siman.h` module of the GNU Scientific Library for the classical simulated annealing subroutine. Parameters were optimised using Bayesian optimisation as in the previous subsection. The probability of success was estimated from a sample of 100 replicas.

#### E. Statistical analysis

We performed a non-linear least squares fit of our data using the *lmfit* library [54]. We considered four functional models: polynomial,  $x^\alpha$ , exponential,  $e^{\alpha x}$ , square exponential,  $e^{\alpha x^2}$  and cubic exponential,  $e^{\alpha x^3}$ . The function was augmented by a constant  $\beta$ , which was set to the average value of the dependent variable for a given length.

We employed three statistical model selection criteria to decide the function that provided the best explanation of the data: the Akaike information criterion (AIC), the Bayesian



information criterion (BIC), and the mean squared error (MSE) of the means. The last method was chosen because of the nature of the dataset: the independent variable is discrete, hence the model only provides the prediction for 4 values (3 in 3D). Thus, understanding how the real means differ from the predicted means provides useful information for model selection.

In addition, in the analysis of quantum annealing and classical simulated annealing data, given the reduced size, we applied an outlier removal procedure: at every length, we kept only datapoints contained in  $\mu \pm 2.5\sigma$ . This procedure was not necessary in the analysis of spectral gap data, given the amount of data.

### Acknowledgments

C. O. would like to thank F. Hoffmann-La Roche, UCB and the UK National Quantum Technologies Programme for financial support through an EPSRC studentship (EP/M013243/1). G. M. M. thanks the EPSRC and MRC for support via EP/L016044/1 and EP/S024093/1. S. C. B. acknowledges support from the EU Flagship project AQTION, the NQIT Hub (EP/M013243/1) and the QCS Hub. The authors would like to thank Daniel Nissley and Niel de Beaudrap for useful discussions.

- 
- [1] D. L. Nelson, A. L. Lehninger, and M. M. Cox, *Lehninger's Principles of Biochemistry*. Macmillan, 2008.
  - [2] S. Jones and J. M. Thornton, "Principles of protein-protein interactions," *Proceedings of the National Academy of Sciences*, vol. 93, no. 1, pp. 13–20, 1996.
  - [3] H. Jhoti and A. R. Leach, *Structure-based Drug Discovery*. Springer, 1 ed., 2007.
  - [4] C. Zeymer and D. Hilvert, "Directed evolution of protein catalysts," *Annual Review of Biochemistry*, vol. 87, pp. 131–157, 2018.
  - [5] T. L. Blundell, "Protein crystallography and drug discovery: recollections of knowledge exchange between academia and industry," *IUCrJ*, vol. 4, no. 4, pp. 308–321, 2017.
  - [6] J.-P. Renaud, A. Chari, C. Ciferri, W.-t. Liu, H.-W. Remigy, H. Stark, and C. Wiesmann, "Cryo-EM in drug discovery: achievements, limitations and prospects," *Nature Reviews Drug*

- Discovery*, vol. 17, no. 7, pp. 471–492, 2018.
- [7] UniProt Consortium, “UniProt: a worldwide hub of protein knowledge,” *Nucleic Acids Research*, vol. 47, no. D1, pp. D506–D515, 2019.
- [8] H. M. Berman, P. E. Bourne, J. Westbrook, and C. Zardecki, “The Protein Data Bank,” in *Protein Structure*, pp. 394–410, CRC Press, 2003.
- [9] J. C. Kendrew, G. Bodo, H. M. Dintzis, R. Parrish, H. Wyckoff, and D. C. Phillips, “A three-dimensional model of the myoglobin molecule obtained by x-ray analysis,” *Nature*, vol. 181, no. 4610, pp. 662–666, 1958.
- [10] K. A. Dill and J. L. MacCallum, “The protein-folding problem, 50 years on,” *Science*, vol. 338, no. 6110, pp. 1042–1046, 2012.
- [11] L. A. Abriata, G. E. Tamò, and M. Dal Peraro, “A further leap of improvement in tertiary structure prediction in casp13 prompts new routes for future assessments,” *Proteins: Structure, Function, and Bioinformatics*, vol. 87, no. 12, pp. 1100–1112, 2019.
- [12] E. Farhi, J. Goldstone, S. Gutmann, and M. Sipser, “Quantum computation by adiabatic evolution,” *arXiv preprint quant-ph/0001106*, 2000.
- [13] M. Born and V. Fock, “Beweis des Adiabatensatzes,” *Zeitschrift für Physik*, vol. 51, no. 3-4, pp. 165–180, 1928.
- [14] K. F. Lau and K. A. Dill, “A lattice statistical mechanics model of the conformational and sequence spaces of proteins,” *Macromolecules*, vol. 22, no. 10, pp. 3986–3997, 1989.
- [15] J. Skolnick, A. Kolinski, D. Kihara, M. Betancourt, P. Rotkiewicz, and M. Boniecki, “Ab initio protein structure prediction via a combination of threading, lattice folding, clustering, and structure refinement,” *Proteins: Structure, Function, and Bioinformatics*, vol. 45, no. S5, pp. 149–156, 2001.
- [16] T. Hoque, M. Chetty, and A. Sattar, “Extended HP model for protein structure prediction,” *Journal of Computational Biology*, vol. 16, no. 1, pp. 85–103, 2009.
- [17] W. E. Hart and S. Istrail, “Robust proofs of NP-hardness for protein folding: general lattices and energy potentials,” *Journal of Computational Biology*, vol. 4, no. 1, pp. 1–22, 1997.
- [18] B. Berger and T. Leighton, “Protein folding in the hydrophobic-hydrophilic (HP) model is NP-complete,” *Journal of Computational Biology*, vol. 5, no. 1, pp. 27–40, 1998.
- [19] A. Perdomo, C. Truncik, I. Tubert-Brohman, G. Rose, and A. Aspuru-Guzik, “Construction of model hamiltonians for adiabatic quantum computation and its application to finding low-

- energy conformations of lattice protein models,” *Physical Review A*, vol. 78, no. 1, p. 012320, 2008.
- [20] R. Babbush, A. Perdomo-Ortiz, B. O’Gorman, W. Macready, and A. Aspuru-Guzik, “Construction of energy functions for lattice heteropolymer models: a case study in constraint satisfaction programming and adiabatic quantum optimization,” *arXiv preprint arXiv:1211.3422*, 2012.
- [21] T. Babej, M. Fingerhuth, *et al.*, “Coarse-grained lattice protein folding on a quantum annealer,” *arXiv preprint arXiv:1811.00713*, 2018.
- [22] A. Perdomo-Ortiz, N. Dickson, M. Drew-Brook, G. Rose, and A. Aspuru-Guzik, “Finding low-energy conformations of lattice protein models by quantum annealing,” *Scientific reports*, vol. 2, p. 571, 2012.
- [23] A. Robert, P. K. Barkoutsos, S. Woerner, and I. Tavernelli, “Resource-efficient quantum algorithm for protein folding,” *arXiv preprint arXiv:1908.02163*, 2019.
- [24] V. K. Mulligan, H. Melo, H. I. Merritt, S. Slocum, B. D. Weitzner, A. M. Watkins, P. D. Renfrew, C. Pelissier, P. S. Arora, and R. Bonneau, “Designing peptides on a quantum computer,” *bioRxiv*, 2019.
- [25] D. A. Lidar, “Towards fault tolerant adiabatic quantum computation,” *Physical Review Letters*, vol. 100, no. 16, p. 160506, 2008.
- [26] K. L. Pudenz, T. Albash, and D. A. Lidar, “Error-corrected quantum annealing with hundreds of qubits,” *Nature Communications*, vol. 5, p. 3243, 2014.
- [27] S. Lloyd, “Universal quantum simulators,” *Science*, vol. 273, pp. 1073–1078, 1996.
- [28] K. A. Dill, S. Bromberg, K. Yue, H. S. Chan, K. M. Ftebig, D. P. Yee, and P. D. Thomas, “Principles of protein folding – a perspective from simple exact models,” *Protein Science*, vol. 4, no. 4, pp. 561–602, 1995.
- [29] T. Albash and D. A. Lidar, “Adiabatic quantum computation,” *Reviews of Modern Physics*, vol. 90, no. 1, p. 015002, 2018.
- [30] W. Van Dam, M. Mosca, and U. Vazirani, “How powerful is adiabatic quantum computation?,” in *Proceedings 42nd IEEE Symposium on Foundations of Computer Science*, pp. 279–287, IEEE, 2001.
- [31] W. van Dam and U. Vazirani, “Limits on quantum adiabatic optimization,” *Unpublished manuscript*, 2001. <https://people.eecs.berkeley.edu/~vazirani/pubs/qao.pdf> Re-

- trieved 10<sup>th</sup> March, 2020.
- [32] B. W. Reichardt, “The quantum adiabatic optimization algorithm and local minima,” in *Proceedings of the thirty-sixth annual ACM symposium on Theory of Computing*, pp. 502–510, ACM, 2004.
- [33] E. Farhi, J. Goldstone, S. Gutmann, J. Lapan, A. Lundgren, and D. Preda, “A quantum adiabatic evolution algorithm applied to random instances of an np-complete problem,” *Science*, vol. 292, no. 5516, pp. 472–475, 2001.
- [34] A. P. Young, S. Knysh, and V. N. Smelyanskiy, “Size dependence of the minimum excitation gap in the quantum adiabatic algorithm,” *Physical Review Letters*, vol. 101, no. 17, p. 170503, 2008.
- [35] A. Young, S. Knysh, and V. Smelyanskiy, “First-order phase transition in the quantum adiabatic algorithm,” *Physical Review Letters*, vol. 104, no. 2, p. 020502, 2010.
- [36] T. F. Rønnow, Z. Wang, J. Job, S. Boixo, S. V. Isakov, D. Wecker, J. M. Martinis, D. A. Lidar, and M. Troyer, “Defining and detecting quantum speedup,” *Science*, vol. 345, no. 6195, pp. 420–424, 2014.
- [37] B. Shahriari, K. Swersky, Z. Wang, R. P. Adams, and N. De Freitas, “Taking the human out of the loop: a review of Bayesian optimization,” *Proceedings of the IEEE*, vol. 104, no. 1, pp. 148–175, 2015.
- [38] The GPyOpt authors, “GPyOpt: a Bayesian optimization framework in Python.” <http://github.com/SheffieldML/GPyOpt>, 2016.
- [39] T. Albash and D. A. Lidar, “Demonstration of a scaling advantage for a quantum annealer over simulated annealing,” *Physical Review X*, vol. 8, no. 3, p. 031016, 2018.
- [40] S. Rajasekaran, “On the convergence time of simulated annealing,” *Technical Reports (CIS)*, p. 356, 1990.
- [41] F. M. Pearl, C. Bennett, J. E. Bray, A. P. Harrison, N. Martin, A. Shepherd, I. Sillitoe, J. Thornton, and C. A. Orengo, “The CATH database: an extended protein family resource for structural and functional genomics,” *Nucleic Acids Research*, vol. 31, no. 1, pp. 452–455, 2003.
- [42] S. Miyazawa and R. L. Jernigan, “Estimation of effective interresidue contact energies from protein crystal structures: quasi-chemical approximation,” *Macromolecules*, vol. 18, no. 3, pp. 534–552, 1985.

- [43] D-Wave Systems, Inc., “D-Wave problem-solving handbook.” [https://docs.dwavesys.com/docs/latest/doc\\_handbook.html](https://docs.dwavesys.com/docs/latest/doc_handbook.html), 2019. Retrieved 10<sup>th</sup> March, 2020.
- [44] O. ertk, “SymEngine.” <https://github.com/symengine/symengine/>, 2012–2020. Retrieved 1<sup>st</sup> April, 2019.
- [45] D-Wave Systems, Inc., “Technical description of the D-Wave quantum processing unit.” [https://docs.dwavesys.com/docs/latest/doc\\_qpu.html](https://docs.dwavesys.com/docs/latest/doc_qpu.html), 2019. Retrieved 10<sup>th</sup> March, 2020.
- [46] T. Albash, “Role of nonstoquastic catalysts in quantum adiabatic optimization,” *Physical Review A*, vol. 99, no. 4, p. 042334, 2019.
- [47] L. Hormozi, E. W. Brown, G. Carleo, and M. Troyer, “Nonstoquastic hamiltonians and quantum annealing of an Ising spin glass,” *Physical Review B*, vol. 95, no. 18, p. 184416, 2017.
- [48] V. Hernández, J. E. Román, A. Tomás, and V. Vidal, “Krylov-Schur methods in SLEPc,” *Universitat Politecnica de Valencia, Tech. Rep. STR-7*, 2007.
- [49] G. W. Stewart, “A Krylov-Schur algorithm for large eigenproblems,” *SIAM Journal on Matrix Analysis and Applications*, vol. 23, no. 3, pp. 601–614, 2002.
- [50] V. Hernandez, J. E. Roman, and V. Vidal, “SLEPc: a scalable and flexible toolkit for the solution of eigenvalue problems,” *ACM Transactions on Mathematical Software (TOMS)*, vol. 31, no. 3, pp. 351–362, 2005.
- [51] S. Abhyankar, J. Brown, E. M. Constantinescu, D. Ghosh, B. F. Smith, and H. Zhang, “PETSc/TS: a modern scalable ODE/DAE solver library,” *arXiv preprint arXiv:1806.01437*, 2018.
- [52] S. Balay, S. Abhyankar, M. Adams, J. Brown, P. Brune, K. Buschelman, L. Dalcin, A. Dener, V. Eijkhout, W. Gropp, *et al.*, “PETSc users manual,” 2019.
- [53] E. Farhi, J. Goldstone, and S. Gutmann, “A numerical study of the performance of a quantum adiabatic evolution algorithm for satisfiability,” *arXiv preprint quant-ph/0007071*, 2000.
- [54] M. Newville, T. Stensitzki, D. B. Allen, M. Rawlik, A. Ingargiola, and A. Nelson, “LMFIT: non-linear least-square minimization and curve-fitting for Python,” *Astrophysics Source Code Library*, 2016.
- [55] Schrödinger, LLC, “The PyMOL molecular graphics system, version 2.4.0a0.” November 2015.

**Appendix A: Model comparison raw data**

Parameter	Model	0-10%	10-25%	25-50%	50-75%	75-90%	90-100%	Full
$\alpha$	$x^\alpha$	$-3.286 \pm 0.053$	$-1.605 \pm 0.012$	$-0.779 \pm 0.005$	$-0.184 \pm 0.005$	$0.148 \pm 0.008$	$0.361 \pm 0.013$	$-0.752 \pm 0.010$
$\alpha$	$e^{\alpha x}$	$-1.598 \pm 0.028$	$-0.781 \pm 0.007$	$-0.379 \pm 0.003$	$-0.088 \pm 0.002$	$0.073 \pm 0.004$	$0.173 \pm 0.007$	$-0.366 \pm 0.005$
$\alpha$	$e^{\alpha x^2}$	$-0.552 \pm 0.012$	$-0.269 \pm 0.003$	$-0.130 \pm 0.001$	$-0.029 \pm 0.001$	$0.025 \pm 0.001$	$0.057 \pm 0.003$	$-0.126 \pm 0.002$
$\alpha$	$e^{\alpha x^3}$	$-0.181 \pm 0.005$	$-0.088 \pm 0.001$	$-0.042 \pm 0.001$	$-0.009 \pm 0.000$	$0.008 \pm 0.001$	$0.018 \pm 0.001$	$-0.041 \pm 0.001$
AIC	$x^\alpha$	<b>2210.30</b>	<b>-2566.22</b>	<b>-9641.00</b>	<b>-9715.92</b>	<b>-4488.14</b>	<b>-2076.36</b>	<b>7421.17</b>
AIC	$e^{\alpha x}$	2381.08	-1849.16	-8455.74	-9587.50	-4474.26	-2016.89	7670.17
AIC	$e^{\alpha x^2}$	2771.33	-540.84	-6273.76	-9297.51	-4429.33	-1884.47	8348.67
AIC	$e^{\alpha x^3}$	3021.55	159.84	-5094.38	-9098.27	-4389.71	-1794.93	8876.53
BIC	$x^\alpha$	<b>2215.63</b>	<b>-2560.49</b>	<b>-9634.76</b>	<b>-9709.68</b>	<b>-4482.41</b>	<b>-2071.03</b>	<b>7428.80</b>
BIC	$e^{\alpha x}$	2386.40	-1843.43	-8449.50	-9581.26	-4468.53	-2011.56	7677.80
BIC	$e^{\alpha x^2}$	2776.65	-535.11	-6267.52	-9291.27	-4423.60	-1879.14	8356.30
BIC	$e^{\alpha x^3}$	3026.87	165.57	-5088.14	-9092.03	-4383.98	-1789.60	8884.15
MSE	$x^\alpha$	22.43548	<b>2.51534</b>	<b>0.20113</b>	<b>1.58745</b>	3.47287	5.09703	<b>0.20860</b>
MSE	$e^{\alpha x}$	20.79187	2.51687	0.39273	1.67794	3.39960	4.83987	0.39967
MSE	$e^{\alpha x^2}$	18.27669	2.74269	0.86278	1.87008	3.23616	4.32081	0.86482
MSE	$e^{\alpha x^3}$	<b>16.62559</b>	2.85132	1.15869	1.99124	<b>3.12596</b>	<b>3.99454</b>	1.15846

TABLE II: Table of statistical fits for the minimum spectral gap between the ground state and the first excited state, for the dataset of 2D protein problems. In bold, we indicate the model preferred by a particular model selection criterion.

Parameter	Model	0-10%	10-25%	25-50%	50-75%	75-90%	90-100%	Full
$\alpha$	$x^\alpha$	$-3.665 \pm 0.051$	$-1.575 \pm 0.011$	$-0.850 \pm 0.004$	$0.391 \pm 0.012$	$1.162 \pm 0.010$	$1.397 \pm 0.015$	$-0.403 \pm 0.014$
$\alpha$	$e^{\alpha x}$	$-2.131 \pm 0.029$	$-0.911 \pm 0.007$	$-0.491 \pm 0.002$	$0.239 \pm 0.007$	$0.680 \pm 0.006$	$0.798 \pm 0.010$	$-0.231 \pm 0.008$
$\alpha$	$e^{\alpha x^2}$	$-1.121 \pm 0.017$	$-0.473 \pm 0.005$	$-0.254 \pm 0.002$	$0.139 \pm 0.004$	$0.363 \pm 0.003$	$0.403 \pm 0.007$	$-0.117 \pm 0.004$
$\alpha$	$e^{\alpha x^3}$	$-0.553 \pm 0.010$	$-0.231 \pm 0.003$	$-0.124 \pm 0.001$	$0.072 \pm 0.002$	$0.180 \pm 0.002$	$0.194 \pm 0.004$	$-0.056 \pm 0.002$
AIC	$x^\alpha$	1021.64	<b>-4169.39</b>	<b>-12803.81</b>	-4379.94	-4437.00	<b>-2481.66</b>	<b>5915.36</b>
AIC	$e^{\alpha x}$	<b>992.01</b>	-4058.99	-12412.42	-4490.25	<b>-4677.59</b>	-2250.96	5936.65
AIC	$e^{\alpha x^2}$	1249.22	-2938.47	-9875.84	-4675.12	-4325.99	-1550.74	6033.55
AIC	$e^{\alpha x^3}$	1510.35	-2213.93	-8464.09	<b>-4729.63</b>	-3775.90	-1173.71	6110.65
BIC	$x^\alpha$	1026.91	<b>-4163.71</b>	<b>-12797.62</b>	-4373.75	-4431.33	<b>-2476.39</b>	<b>5922.93</b>
BIC	$e^{\alpha x}$	<b>997.28</b>	-4053.32	-12406.23	-4484.06	<b>-4671.92</b>	-2245.69	5944.22
BIC	$e^{\alpha x^2}$	1254.49	-2932.80	-9869.66	-4668.93	-4320.32	-1545.48	6041.12
BIC	$e^{\alpha x^3}$	1515.61	-2208.26	-8457.91	<b>-4723.44</b>	-3770.23	-1168.44	6118.22
MSE	$x^\alpha$	17.94229	2.31403	<b>0.33712</b>	<b>1.06890</b>	4.14115	5.47780	<b>0.00191</b>
MSE	$e^{\alpha x}$	18.05314	2.31351	0.34474	1.11557	4.16563	5.31365	0.00912
MSE	$e^{\alpha x^2}$	17.15902	2.18661	0.35862	1.16065	3.96442	4.65149	0.04226
MSE	$e^{\alpha x^3}$	<b>16.05752</b>	<b>2.05104</b>	0.36410	1.14990	<b>3.71657</b>	<b>4.14621</b>	0.06887

TABLE III: Table of statistical fits for the minimum spectral gap between the ground state and the first excited state, for the dataset of 3D protein problems. In bold, we indicate the model preferred by a particular model selection criterion.



Parameter	Model	0-10%	10-25%	25-50%	50-75%	75-90%	90-100%	Full
$\alpha$	$x^\alpha$	$0.031 \pm 0.058$	$0.265 \pm 0.026$	$0.460 \pm 0.010$	$0.795 \pm 0.015$	$1.107 \pm 0.027$	$1.510 \pm 0.060$	$0.672 \pm 0.025$
$\alpha$	$e^{\alpha x}$	$0.009 \pm 0.013$	$0.059 \pm 0.006$	$0.101 \pm 0.002$	$0.176 \pm 0.003$	$0.245 \pm 0.005$	$0.333 \pm 0.013$	$0.149 \pm 0.005$
$\alpha$	$e^{\alpha x^2}$	$0.005 \pm 0.005$	$0.022 \pm 0.002$	$0.036 \pm 0.002$	$0.064 \pm 0.002$	$0.089 \pm 0.004$	$0.120 \pm 0.008$	$0.054 \pm 0.002$
$\alpha$	$e^{\alpha x^3}$	$0.002 \pm 0.002$	$0.007 \pm 0.001$	$0.012 \pm 0.001$	$0.021 \pm 0.001$	$0.030 \pm 0.002$	$0.040 \pm 0.003$	$0.018 \pm 0.001$
AIC	$x^\alpha$	-149.70	-287.88	<b>-612.57</b>	-527.89	-276.94	<b>-147.00</b>	-1240.01
AIC	$e^{\alpha x}$	-149.96	<b>-288.86</b>	-592.28	<b>-533.08</b>	<b>-287.01</b>	-145.83	<b>-1243.19</b>
AIC	$e^{\alpha x^2}$	-150.45	-281.14	-491.06	-409.62	-213.34	-112.17	-1186.99
AIC	$e^{\alpha x^3}$	<b>-150.55</b>	-272.31	-442.33	-352.09	-178.27	-93.24	-1129.40
BIC	$x^\alpha$	-148.01	-285.82	<b>-610.01</b>	-525.35	-274.91	<b>-145.31</b>	-1236.06
BIC	$e^{\alpha x}$	-148.27	<b>-286.80</b>	-589.71	<b>-530.54</b>	<b>-284.98</b>	-144.14	<b>-1239.24</b>
BIC	$e^{\alpha x^2}$	-148.76	-279.08	-488.49	-407.08	-211.31	-110.48	-1183.04
BIC	$e^{\alpha x^3}$	<b>-148.86</b>	-270.25	-439.76	-349.55	-176.24	-91.55	-1125.45
MSE	$x^\alpha$	0.28234	0.11476	0.03290	0.01252	0.13092	0.48034	0.00226
MSE	$e^{\alpha x}$	0.27206	<b>0.11299</b>	<b>0.03275</b>	<b>0.01143</b>	<b>0.13057</b>	0.47586	<b>0.00097</b>
MSE	$e^{\alpha x^2}$	<b>0.26061</b>	0.12761	0.05664	0.03512	0.14624	0.45802	0.02540
MSE	$e^{\alpha x^3}$	0.26128	0.14645	0.08373	0.06295	0.16469	<b>0.44568</b>	0.05436

TABLE IV: Table of statistical fits for the expected quantum annealing runtime for the worst-case dataset in 2D. In bold, we indicate the model preferred by a particular model selection criterion.

Parameter	Model	0-10%	10-25%	25-50%	50-75%	75-90%	90-100%	Full
$\alpha$	$x^\alpha$	$0.197 \pm 0.034$	$0.313 \pm 0.025$	$0.497 \pm 0.017$	$0.728 \pm 0.015$	$0.928 \pm 0.033$	$1.294 \pm 0.065$	$0.642 \pm 0.020$
$\alpha$	$e^{\alpha x}$	$0.046 \pm 0.007$	$0.071 \pm 0.005$	$0.111 \pm 0.004$	$0.161 \pm 0.004$	$0.203 \pm 0.009$	$0.282 \pm 0.017$	$0.142 \pm 0.004$
$\alpha$	$e^{\alpha x^2}$	$0.018 \pm 0.003$	$0.027 \pm 0.002$	$0.041 \pm 0.002$	$0.058 \pm 0.002$	$0.073 \pm 0.005$	$0.099 \pm 0.009$	$0.052 \pm 0.002$
$\alpha$	$e^{\alpha x^3}$	$0.006 \pm 0.001$	$0.009 \pm 0.001$	$0.014 \pm 0.001$	$0.020 \pm 0.001$	$0.024 \pm 0.002$	$0.033 \pm 0.004$	$0.017 \pm 0.001$
AIC	$x^\alpha$	-186.48	-282.65	-491.03	<b>-514.65</b>	<b>-248.51</b>	<b>-137.01</b>	<b>-1357.19</b>
AIC	$e^{\alpha x}$	-190.18	<b>-290.24</b>	<b>-499.15</b>	-501.84	-231.11	-125.93	-1351.74
AIC	$e^{\alpha x^2}$	<b>-193.61</b>	-289.73	-456.11	-402.68	-186.83	-98.81	-1274.09
AIC	$e^{\alpha x^3}$	-192.53	-281.21	-424.12	-358.44	-166.78	-86.11	-1212.57
BIC	$x^\alpha$	-184.84	-280.66	-488.53	<b>-512.15</b>	<b>-246.54</b>	<b>-135.37</b>	<b>-1353.30</b>
BIC	$e^{\alpha x}$	-188.54	<b>-288.25</b>	<b>-496.65</b>	-499.34	-229.14	-124.29	-1347.85
BIC	$e^{\alpha x^2}$	<b>-191.97</b>	-287.74	-453.61	-400.18	-184.86	-97.17	-1270.20
BIC	$e^{\alpha x^3}$	-190.89	-279.22	-421.62	-355.94	-164.81	-84.47	-1208.68
MSE	$x^\alpha$	0.14249	0.08153	<b>0.02162</b>	<b>0.01197</b>	0.06227	0.29482	<b>0.00706</b>
MSE	$e^{\alpha x}$	<b>0.13655</b>	<b>0.07829</b>	0.02171	0.01340	<b>0.06107</b>	0.28277	0.00824
MSE	$e^{\alpha x^2}$	0.13927	0.08846	0.04172	0.03587	0.07512	0.25662	0.03091
MSE	$e^{\alpha x^3}$	0.14835	0.10230	0.06192	0.05742	0.09064	<b>0.24276</b>	0.05290

TABLE V: Table of statistical fits for the expected quantum annealing runtime for the random dataset in 2D. In bold, we indicate the model preferred by a particular model selection criterion.

Parameter	Model	0-10%	10-25%	25-50%	50-75%	75-90%	90-100%	Full
$\alpha$	$x^\alpha$	$1.241 \pm 0.137$	$1.344 \pm 0.096$	$1.491 \pm 0.055$	$1.773 \pm 0.021$	$2.002 \pm 0.053$	$2.343 \pm 0.171$	$1.676 \pm 0.036$
$\alpha$	$e^{\alpha x}$	$0.329 \pm 0.029$	$0.351 \pm 0.019$	$0.384 \pm 0.010$	$0.445 \pm 0.006$	$0.496 \pm 0.019$	$0.571 \pm 0.052$	$0.424 \pm 0.009$
$\alpha$	$e^{\alpha x^2}$	$0.191 \pm 0.010$	$0.198 \pm 0.006$	$0.211 \pm 0.003$	$0.231 \pm 0.008$	$0.250 \pm 0.018$	$0.274 \pm 0.039$	$0.224 \pm 0.006$
$\alpha$	$e^{\alpha x^3}$	$0.099 \pm 0.004$	$0.102 \pm 0.002$	$0.107 \pm 0.002$	$0.113 \pm 0.006$	$0.120 \pm 0.011$	$0.127 \pm 0.023$	$0.111 \pm 0.003$
AIC	$x^\alpha$	-83.43	-137.51	-276.34	<b>-412.16</b>	<b>-189.25</b>	<b>-70.28</b>	-937.74
AIC	$e^{\alpha x}$	-93.59	-156.59	-324.99	-391.41	-158.26	-59.27	<b>-961.33</b>
AIC	$e^{\alpha x^2}$	-122.89	-212.15	<b>-408.62</b>	-258.19	-109.09	-40.07	-874.59
AIC	$e^{\alpha x^3}$	<b>-138.75</b>	<b>-227.55</b>	-343.24	-213.18	-90.80	-32.14	-785.15
BIC	$x^\alpha$	-82.03	-135.73	-274.04	<b>-409.87</b>	<b>-187.46</b>	<b>-68.88</b>	-934.05
BIC	$e^{\alpha x}$	-92.19	-154.81	-322.69	-389.12	-156.47	-57.87	<b>-957.64</b>
BIC	$e^{\alpha x^2}$	-121.49	-210.37	<b>-406.31</b>	-255.90	-107.31	-38.67	-870.91
BIC	$e^{\alpha x^3}$	<b>-137.35</b>	<b>-225.77</b>	-340.93	-210.89	-89.02	-30.74	-781.46
MSE	$x^\alpha$	0.06899	0.04407	0.02023	0.01300	0.04434	0.15289	0.00975
MSE	$e^{\alpha x}$	<b>0.04570</b>	<b>0.02694</b>	<b>0.00800</b>	<b>0.00221</b>	<b>0.02562</b>	0.10706	<b>0.00002</b>
MSE	$e^{\alpha x^2}$	0.06041	0.05259	0.04358	0.04114	0.05080	<b>0.08194</b>	0.04043
MSE	$e^{\alpha x^3}$	0.10648	0.10266	0.09807	0.09714	0.10178	0.11401	0.09681

TABLE VI: Table of statistical fits for the expected quantum annealing runtime for the worst-case dataset in 3D. In bold, we indicate the model preferred by a particular model selection criterion.

Parameter	Model	0-10%	10-25%	25-50%	50-75%	75-90%	90-100%	Full
$\alpha$	$x^\alpha$	$1.644 \pm 0.122$	$1.733 \pm 0.091$	$1.816 \pm 0.060$	$1.942 \pm 0.054$	$2.200 \pm 0.035$	$2.815 \pm 0.175$	$1.978 \pm 0.038$
$\alpha$	$e^{\alpha x}$	$0.429 \pm 0.023$	$0.448 \pm 0.016$	$0.469 \pm 0.010$	$0.499 \pm 0.008$	$0.554 \pm 0.007$	$0.688 \pm 0.055$	$0.504 \pm 0.008$
$\alpha$	$e^{\alpha x^2}$	$0.241 \pm 0.004$	$0.248 \pm 0.002$	$0.258 \pm 0.002$	$0.272 \pm 0.003$	$0.290 \pm 0.012$	$0.334 \pm 0.043$	$0.271 \pm 0.005$
$\alpha$	$e^{\alpha x^3}$	$0.123 \pm 0.002$	$0.126 \pm 0.002$	$0.130 \pm 0.003$	$0.136 \pm 0.004$	$0.143 \pm 0.009$	$0.156 \pm 0.025$	$0.135 \pm 0.003$
AIC	$x^\alpha$	-90.49	-142.04	-256.61	-272.30	-221.56	<b>-69.03</b>	-903.10
AIC	$e^{\alpha x}$	-107.31	-170.90	-319.80	-349.58	<b>-236.72</b>	-55.79	<b>-975.92</b>
AIC	$e^{\alpha x^2}$	<b>-170.86</b>	<b>-283.27</b>	<b>-491.91</b>	<b>-395.21</b>	-142.57	-33.77	-920.09
AIC	$e^{\alpha x^3}$	-166.46	-230.03	-325.45	-283.26	-112.39	-24.94	-803.86
BIC	$x^\alpha$	-89.09	-140.26	-254.34	-270.02	-219.80	<b>-67.63</b>	-899.42
BIC	$e^{\alpha x}$	-105.91	-169.11	-317.52	-347.30	<b>-234.96</b>	-54.39	<b>-972.24</b>
BIC	$e^{\alpha x^2}$	<b>-169.46</b>	<b>-281.48</b>	<b>-489.63</b>	<b>-392.93</b>	-140.81	-32.37	-916.41
BIC	$e^{\alpha x^3}$	-165.05	-228.24	-323.18	-280.98	-110.63	-23.54	-800.19
MSE	$x^\alpha$	0.07051	0.05430	0.04381	0.03617	0.05208	0.26086	0.03583
MSE	$e^{\alpha x}$	<b>0.03439</b>	<b>0.02162</b>	<b>0.01238</b>	<b>0.00623</b>	<b>0.01876</b>	0.17519	<b>0.00609</b>
MSE	$e^{\alpha x^2}$	0.04346	0.03699	0.03132	0.02834	0.03476	<b>0.09525</b>	0.02834
MSE	$e^{\alpha x^3}$	0.10002	0.09602	0.09251	0.09105	0.09499	0.11941	0.09093

TABLE VII: Table of statistical fits for the expected quantum annealing runtime for the random dataset in 3D. In bold, we indicate the model preferred by a particular model selection criterion.

Parameter	Model	0-10%	10-25%	25-50%	50-75%	75-90%	90-100%	Full
$\alpha$	$x^\alpha$	$0.342 \pm 0.024$	$0.370 \pm 0.022$	$0.406 \pm 0.017$	$0.441 \pm 0.019$	$0.474 \pm 0.027$	$0.582 \pm 0.043$	$0.431 \pm 0.010$
$\alpha$	$e^{\alpha x}$	$0.079 \pm 0.004$	$0.086 \pm 0.003$	$0.094 \pm 0.003$	$0.102 \pm 0.003$	$0.110 \pm 0.004$	$0.134 \pm 0.007$	$0.100 \pm 0.002$
$\alpha$	$e^{\alpha x^2}$	$0.031 \pm 0.000$	$0.034 \pm 0.000$	$0.037 \pm 0.000$	$0.040 \pm 0.000$	$0.043 \pm 0.000$	$0.053 \pm 0.001$	$0.039 \pm 0.000$
$\alpha$	$e^{\alpha x^3}$	$0.011 \pm 0.000$	$0.012 \pm 0.000$	$0.013 \pm 0.000$	$0.014 \pm 0.000$	$0.015 \pm 0.000$	$0.019 \pm 0.000$	$0.014 \pm 0.000$
AIC	$x^\alpha$	-221.09	-302.58	-502.23	-484.59	-281.00	-174.66	-1909.64
AIC	$e^{\alpha x}$	-249.38	-343.60	-575.55	-558.84	-325.25	-199.98	-2139.47
AIC	$e^{\alpha x^2}$	<b>-368.49</b>	<b>-553.71</b>	<b>-956.21</b>	<b>-866.85</b>	<b>-525.90</b>	<b>-270.71</b>	<b>-2608.48</b>
AIC	$e^{\alpha x^3}$	-320.65	-436.13	-692.79	-647.66	-380.99	-253.89	-2428.29
BIC	$x^\alpha$	-219.40	-300.56	-499.68	-482.06	-278.97	-172.97	-1905.70
BIC	$e^{\alpha x}$	-247.69	-341.57	-573.00	-556.31	-323.22	-198.29	-2135.53
BIC	$e^{\alpha x^2}$	<b>-366.80</b>	<b>-551.68</b>	<b>-953.67</b>	<b>-864.31</b>	<b>-523.87</b>	<b>-269.02</b>	<b>-2604.55</b>
BIC	$e^{\alpha x^3}$	-318.96	-434.11	-690.25	-645.13	-378.96	-252.20	-2424.35
MSE	$x^\alpha$	0.02763	0.02468	0.02233	0.02179	0.02282	0.03639	0.02177
MSE	$e^{\alpha x}$	0.01633	0.01286	0.01063	0.01007	0.01142	0.02644	0.01005
MSE	$e^{\alpha x^2}$	<b>0.00662</b>	<b>0.00264</b>	<b>0.00075</b>	<b>0.00016</b>	<b>0.00190</b>	<b>0.01857</b>	<b>0.00013</b>
MSE	$e^{\alpha x^3}$	0.00883	0.00492	0.00325	0.00266	0.00440	0.02136	0.00264

TABLE VIII: Table of statistical fits for the expected number of energy evaluations in classical simulated annealing for the worst-case dataset in 2D. In bold, we indicate the model preferred by a particular model selection criterion.

Parameter	Model	0-10%	10-25%	25-50%	50-75%	75-90%	90-100%	Full
$\alpha$	$x^\alpha$	$0.291 \pm 0.022$	$0.330 \pm 0.020$	$0.366 \pm 0.017$	$0.404 \pm 0.019$	$0.450 \pm 0.027$	$0.585 \pm 0.046$	$0.397 \pm 0.010$
$\alpha$	$e^{\alpha x}$	$0.068 \pm 0.003$	$0.077 \pm 0.003$	$0.085 \pm 0.003$	$0.094 \pm 0.003$	$0.105 \pm 0.004$	$0.136 \pm 0.008$	$0.092 \pm 0.002$
$\alpha$	$e^{\alpha x^2}$	$0.027 \pm 0.000$	$0.030 \pm 0.000$	$0.034 \pm 0.000$	$0.037 \pm 0.000$	$0.041 \pm 0.000$	$0.054 \pm 0.001$	$0.036 \pm 0.000$
$\alpha$	$e^{\alpha x^3}$	$0.009 \pm 0.000$	$0.011 \pm 0.000$	$0.012 \pm 0.000$	$0.013 \pm 0.000$	$0.014 \pm 0.000$	$0.019 \pm 0.001$	$0.013 \pm 0.000$
AIC	$x^\alpha$	-220.91	-308.49	-481.97	-467.88	-261.99	-163.71	-1819.85
AIC	$e^{\alpha x}$	-247.33	-347.44	-544.89	-532.60	-299.81	-186.41	-2004.83
AIC	$e^{\alpha x^2}$	<b>-349.17</b>	<b>-530.83</b>	<b>-832.72</b>	<b>-839.80</b>	<b>-481.49</b>	<b>-239.03</b>	<b>-2348.93</b>
AIC	$e^{\alpha x^3}$	-312.87	-457.07	-720.89	-688.38	-383.29	-225.58	-2278.73
BIC	$x^\alpha$	-219.27	-306.49	-479.48	-465.39	-260.04	-162.07	-1815.96
BIC	$e^{\alpha x}$	-245.69	-345.43	-542.41	-530.11	-297.86	-184.77	-2000.94
BIC	$e^{\alpha x^2}$	<b>-347.53</b>	<b>-528.83</b>	<b>-830.23</b>	<b>-837.31</b>	<b>-479.54</b>	<b>-237.39</b>	<b>-2345.04</b>
BIC	$e^{\alpha x^3}$	-311.24	-455.06	-718.40	-685.89	-381.34	-223.94	-2274.85
MSE	$x^\alpha$	0.02863	0.02382	0.02123	0.02035	0.02197	0.04334	0.02036
MSE	$e^{\alpha x}$	0.01860	0.01347	0.01070	0.00984	0.01178	0.03607	0.00983
MSE	$e^{\alpha x^2}$	<b>0.00937</b>	<b>0.00395</b>	<b>0.00104</b>	<b>0.00024</b>	<b>0.00262</b>	<b>0.02961</b>	<b>0.00022</b>
MSE	$e^{\alpha x^3}$	0.01056	0.00520	0.00234	0.00158	0.00403	0.03065	0.00156

TABLE IX: Table of statistical fits for the expected number of energy evaluations in classical simulated annealing for the random dataset in 2D. In bold, we indicate the model preferred by a particular model selection criterion.

Parameter	Model	0-10%	10-25%	25-50%	50-75%	75-90%	90-100%	Full
$\alpha$	$x^\alpha$	$0.331 \pm 0.024$	$0.359 \pm 0.020$	$0.395 \pm 0.017$	$0.439 \pm 0.019$	$0.464 \pm 0.026$	$0.493 \pm 0.032$	$0.414 \pm 0.009$
$\alpha$	$e^{\alpha x}$	$0.086 \pm 0.004$	$0.093 \pm 0.004$	$0.103 \pm 0.003$	$0.114 \pm 0.004$	$0.121 \pm 0.005$	$0.128 \pm 0.006$	$0.108 \pm 0.002$
$\alpha$	$e^{\alpha x^2}$	$0.048 \pm 0.001$	$0.052 \pm 0.000$	$0.057 \pm 0.000$	$0.064 \pm 0.000$	$0.068 \pm 0.000$	$0.071 \pm 0.000$	$0.060 \pm 0.000$
$\alpha$	$e^{\alpha x^3}$	$0.025 \pm 0.000$	$0.027 \pm 0.000$	$0.029 \pm 0.000$	$0.032 \pm 0.000$	$0.034 \pm 0.000$	$0.036 \pm 0.001$	$0.031 \pm 0.000$
AIC	$x^\alpha$	-189.03	-266.65	-437.52	-414.11	-250.89	-164.34	-1697.35
AIC	$e^{\alpha x}$	-207.15	-294.11	-483.51	-459.26	-278.90	-184.10	-1856.48
AIC	$e^{\alpha x^2}$	<b>-295.05</b>	<b>-454.12</b>	<b>-717.37</b>	<b>-714.97</b>	<b>-444.30</b>	<b>-310.68</b>	<b>-2316.48</b>
AIC	$e^{\alpha x^3}$	-276.28	-384.31	-622.73	-613.55	-373.74	-230.00	-2217.73
BIC	$x^\alpha$	-187.63	-264.89	-435.24	-411.84	-249.11	-162.98	-1693.68
BIC	$e^{\alpha x}$	-205.74	-292.35	-481.23	-457.00	-277.12	-182.73	-1852.81
BIC	$e^{\alpha x^2}$	<b>-293.65</b>	<b>-452.36</b>	<b>-715.09</b>	<b>-712.71</b>	<b>-442.52</b>	<b>-309.31</b>	<b>-2312.81</b>
BIC	$e^{\alpha x^3}$	-274.88	-382.54	-620.45	-611.29	-371.95	-228.64	-2214.06
MSE	$x^\alpha$	0.00943	0.00824	0.00740	0.00752	0.00813	0.00933	0.00730
MSE	$e^{\alpha x}$	0.00607	0.00484	0.00396	0.00405	0.00473	0.00595	0.00384
MSE	$e^{\alpha x^2}$	<b>0.00239</b>	<b>0.00113</b>	<b>0.00022</b>	<b>0.00027</b>	<b>0.00102</b>	<b>0.00221</b>	<b>0.00007</b>
MSE	$e^{\alpha x^3}$	0.00274	0.00152	0.00062	0.00066	0.00142	0.00253	0.00046

TABLE X: Table of statistical fits for the expected number of energy evaluations in classical simulated annealing for the worst-case dataset in 3D. In bold, we indicate the model preferred by a particular model selection criterion.

Parameter	Model	0-10%	10-25%	25-50%	50-75%	75-90%	90-100%	Full
$\alpha$	$x^\alpha$	$0.307 \pm 0.022$	$0.350 \pm 0.020$	$0.393 \pm 0.018$	$0.434 \pm 0.018$	$0.471 \pm 0.025$	$0.511 \pm 0.031$	$0.412 \pm 0.009$
$\alpha$	$e^{\alpha x}$	$0.080 \pm 0.004$	$0.091 \pm 0.004$	$0.102 \pm 0.003$	$0.113 \pm 0.003$	$0.122 \pm 0.005$	$0.132 \pm 0.005$	$0.107 \pm 0.002$
$\alpha$	$e^{\alpha x^2}$	$0.045 \pm 0.001$	$0.051 \pm 0.000$	$0.057 \pm 0.000$	$0.063 \pm 0.000$	$0.068 \pm 0.000$	$0.074 \pm 0.000$	$0.060 \pm 0.001$
$\alpha$	$e^{\alpha x^3}$	$0.023 \pm 0.000$	$0.026 \pm 0.000$	$0.029 \pm 0.000$	$0.032 \pm 0.000$	$0.035 \pm 0.001$	$0.037 \pm 0.001$	$0.030 \pm 0.000$
AIC	$x^\alpha$	-193.22	-279.36	-438.15	-432.59	-254.52	-172.20	-1732.82
AIC	$e^{\alpha x}$	-211.13	-306.42	-482.39	-480.03	-284.26	-193.96	-1887.22
AIC	$e^{\alpha x^2}$	<b>-293.47</b>	<b>-436.46</b>	<b>-705.67</b>	<b>-746.36</b>	<b>-458.90</b>	<b>-326.59</b>	<b>-2286.23</b>
AIC	$e^{\alpha x^3}$	-278.35	-410.57	-663.73	-621.05	-354.01	-228.19	-2204.57
BIC	$x^\alpha$	-191.81	-277.55	-435.86	-430.30	-252.74	-170.80	-1729.13
BIC	$e^{\alpha x}$	-209.72	-304.61	-480.10	-477.74	-282.48	-192.56	-1883.53
BIC	$e^{\alpha x^2}$	<b>-292.07</b>	<b>-434.65</b>	<b>-703.38</b>	<b>-744.07</b>	<b>-457.12</b>	<b>-325.18</b>	<b>-2282.54</b>
BIC	$e^{\alpha x^3}$	-276.95	-408.77	-661.44	-618.76	-352.23	-226.79	-2200.88
MSE	$x^\alpha$	0.01053	0.00830	0.00723	0.00732	0.00830	0.01037	0.00714
MSE	$e^{\alpha x}$	0.00731	0.00495	0.00384	0.00391	0.00495	0.00705	0.00374
MSE	$e^{\alpha x^2}$	<b>0.00378</b>	<b>0.00130</b>	<b>0.00017</b>	<b>0.00021</b>	<b>0.00128</b>	<b>0.00333</b>	<b>0.00006</b>
MSE	$e^{\alpha x^3}$	0.00413	0.00168	0.00057	0.00062	0.00165	0.00359	0.00047

TABLE XI: Table of statistical fits for the expected number of energy evaluations in classical simulated annealing for the random dataset in 3D. In bold, we indicate the model preferred by a particular model selection criterion.